The perfect pattern of moisture transport for precipitation for Arctic sea ice melting

Luis Gimeno-Sotelo[1], Raquel Nieto[2], Marta Vázquez[2], Luis Gimeno[2]

[1]Facultade de Matemáticas, Universidade de Santiago de Compostela, 15782 Spain.

5   [2]Environmental Physics Laboratory (EphysLab), Universidade de Vigo, Ourense, 32004, Spain

Correspondence to: Luis Gimeno (l.gimeno@uvigo.es)

Abstract. We have identified the patterns of moisture transport for precipitation over the Arctic region, the Arctic Ocean, and its 13 main subdomains, which better fit with sea ice decline. For this purpose, we studied the different patterns of moisture transport for the case of high/low Arctic sea ice (ASI) extension linked to periods before/after the main change point (CP) in

10   the extension of sea ice. The pattern consists of a general decrease in moisture transport in summer and enhanced moisture transport in autumn and early winter, with different contributions depending on the moisture source and ocean subregion. The pattern is not only statistically significant but also consistent with Eulerian fluxes diagnosis, changes in the frequency of circulation types, and known mechanisms of the effects of snowfall or rainfall on ice in the Arctic. The results of this paper also reveal that the assumed and partially documented enhanced poleward moisture transport from lower latitudes as a

15   consequence of increased moisture from climate change seems to be less simple and constant than typically recognized in relation to enhanced Arctic precipitation throughout the year in the present climate.

1 Introduction

The shrinking of the cryosphere since the 1970s is among the most robust signals of climate change identified in the last IPCC

20   Assessment *(IPCC, 2013)*. There is little doubt that this change is a result of global warming caused by increased anthropogenic greenhouse gas emissions *(AR5; IPCC, 2013)*. The Arctic is of particular scientific and environmental interest; the rise in Arctic near-surface temperature doubles the global average in almost all months *(e.g., Screen and Simmonds, 2010; Tang et al., 2014, Cohen et al., 2014)*. Without doubt, the most important indicator of Arctic climate change is sea ice extent, which is characterised by a very significant decline since the 1970s *(Tang et al., 2014; IPCC, 2013)*. This decline has accelerated in

25   recent decades in terms of both extent and thickness to the point where a summer ice-free Arctic Ocean is expected to occur within the next few decades *(IPCC, 2013)*. Changes in atmospheric and oceanic circulation with implications for Arctic mid-latitude climate or reductions and shifts in the distribution of oceanic and terrestrial fauna are among the most concerning and already apparent impacts of this decline in sea ice (Screen and Simmonds, 2010; Post et al, 2013).The scientific mechanisms involved in Arctic sea ice extension (SIE) are multiple and varied; atmospheric processes *(Ogi and Wallace, 2007; Rigor et*

al., 2002) interact closely and nonlinearly with hydrological and oceanographic processes *(Zhang et al.,1999; Årthun et al., 2012; Zhang et al., 2012)*. Changes in atmospheric circulation can affect SIE via dynamical (e.g. changes of surface winds) or thermodynamic factors (i.e. changes in heat and moisture fluxes in the Arctic *(Tjernström et al., 2015; Ding et al., 2017).*ong these effects, change in moisture transport has emerged as one of the most important with respect to the greenhouse effect

5 *(Koenigk et al., 2013; Graversen and Burtu, 2016, Vihma, 2016)*, and is related to SIE decline through hydrological mechanisms such as changes in Arctic river discharges *(Zhang et al., 2012)*, radiative mechanisms such as anomalous downward longwave radiation at the surface *(Woods et al., 2013; Park et al., 2015a; Mortin et al., 2016; Woods and Caballero, 2016, Lee et al., 2017)*, or meteorological mechanisms such as changes in the frequency and intensity of cyclones crossing the Arctic *(Rinke et al., 2017)*. Because the effects of enhanced moisture transport on Arctic ice are diverse, there is no direct

10 relationship between enhanced transport and SIE decline. Anomalously high moisture transport into the Arctic is associated with intense surface winds, and increment in moisture content and induced radiative warming, which lead to decreased SIE *(Kapsch et al., 2013; Park et al., 2015b)*. However, anomalous moisture transport can result in anomalous precipitation, and in this case, the relation between enhanced moisture transport and diminished SIE is unclear because changes in precipitation are not always related to SIE in the same way, depending on the type of precipitation and the season. Snowfall on sea ice

15 enhances thermal insulation and thus reduces sea ice growth in winter *(Leppäranta, 1993)*, but increases the surface albedo and thus reduces melt in spring and summer *(Cheng et al., 2008)*. In contrast, rainfall is generally related to sea ice melt, and for both snowfall and rainfall, flooding over the ice favours the formation of superimposed ice and potentially increases in the Arctic sea ice thickness.

In this article, we focus on identifying the patterns of moisture transport for precipitation in the Arctic region (AR), the Arctic

20 Ocean (AO) as a whole, and its 13 main subdomains, which fit better with sea ice decline. For this purpose, we have studied the different patterns of moisture transport for the cases of high and low SIE linked to periods before and after the main change point (CP) in the extension of sea ice.

2 Data and Methods

2.1 Data

The target region in this study comprises the AR (figure 1a) as defined by Roberts et al. (2010) and used by *Vazquez et al. (2016)*, the AO as a whole, and its 13 main subdomains as defined in figure 1b (Boisvert et al., 2015). The analysed period was from 1 January 1980 to 31 December 2016. For Arctic SIE, we used daily, monthly and annual data from the U.S. National Snow and Ice Data Center (Fetterer, 2016), and to implement the Lagrangian approach, by which moisture transport is

30 estimated to approximate vertical integrated moisture fluxes and circulation types, we used the European Centre for Medium-Range Weather Forecasts (ECMWF) interim Re-Analysis (ERA-Interim) *(Dee et al., 2011)*. Data from this reanalysis cover

the period from January 1979 to the present and extending forward continuously in near-real time. These data are available at six-hour intervals at a 1° x 1° spatial resolution in latitude and longitude for 61 vertical levels (1000 to 0.1 hPa). The ERA-Interim reanalysis is typically considered to have the highest quality relative to other reanalysis data for the water cycle *(Lorenz and Kunstmann, 2012)* and is especially appropriate over the Arctic region *(Jakobson et al., 2012),* with better representation

5   of mass fluxes including water vapor *(Graversen et al., 2011)*.

2.2 Methods

2.2.1 Calculation of sea ice extension anomalies

Daily, monthly and annual data of sea ice extension from 1980 to 2016 taken from the National Snow and Ice Data Center

10   *(Fetterer, 2016)* were used to build four different series of ice extension anomalies for the whole Arctic Ocean (AO) and its 13 subregions. These four series were constructed as follows:

DS: 365 daily anomaly series (size of each series: 37 data points); for each daily value, the average for the same calendar day over the 37-year period is subtracted (for instance, the series for 21 September comprises the anomaly of each 21 September vs. the average of the 37 data points from this date)

15   **MS:** 12 monthly anomaly series (size of each series: 37 data points); for each monthly value, the average for the same month over the 37-year period is subtracted (for instance the series for September results of the anomaly of each September vs the average of the 37 September data points).

ADS: one series of all daily anomalies (size of the series: 13,505 data points) built by ordering the daily anomalies in DS from 1 January 1980 to 31 December 2016.

20   **AMS:** one series of all monthly anomalies (size of the series: 444 data points) built by ordering the monthly anomalies in MS from January 1980 to December 2016.

2.2.2 Detection of change points in Arctic sea ice extension

Change points of each of these series for the AO were calculated using three different methods, one detecting single change

25   points (At Most One Change, AMOC) and two detecting multiple change points (BinSeg and PELT).

AMOC uses employs a test to detect a hypothesised single change point (CP). The null hypothesis refers to no change point, and its maximum log-likelihood is given by $\boldsymbol{log\ p}\left(\boldsymbol{y_{1:n}}|\widehat{\boldsymbol{\theta_1}}\right)$, where p($\cdot$) is the probability density function associated with the distribution of the data and $\widehat{\boldsymbol{\theta}}$ is the maximum likelihood estimate of the parameters. For the alternative hypothesis, a change point at $\boldsymbol{\tau_1}$ is considered, with $\boldsymbol{\tau_1} \in \{\boldsymbol{1, 2, ..., n-1}\}$. The expression for the maximum log-likelihood for a given $\boldsymbol{\tau_1}$ is

30   $$ML(\tau_1) = \log p\left(y_{1:\tau_1}|\widehat{\theta_1}\right) + \log p\left(y_{(\tau_1+1):n}|\widehat{\theta_2}\right).$$

Taking into account that the CP location is discrete in nature, $\max \tau_1 \, ML(\tau_1)$ is the maximum log-likelihood value under the alternative hypothesis, where the maximum is taken over all possible change-point locations. Consequently, the test statistic is $\lambda = 2[\max \tau_1 \, ML(\tau_1) - \log p(y_{1:n}|\widehat{\theta})]$. The null hypothesis is rejected if $\lambda > C^*$, where C^* is a threshold of our choice. When detecting a CP, its position is estimated as $\widehat{\tau_1}$, which is the value of $\widehat{\tau_1}$ that maximises $ML(\tau_1)$.

5 BinSeg and PELT: by summing the likelihood for each of the m segments, the likelihood test statistic can be extended to multiple changes. However, there is a problem in identifying the maximum of $ML(\tau_{1:m})$ over all possible combinations of $\tau_{1:m}$. The most common approach to resolve this problem is to minimise

$$\sum_{i=1}^{m+1}[C(y_{(\tau_{i-1}+1):\tau_i})] + \beta f(m) \; (1)$$

where C^* is a cost function for a segment, such as the negative log-likelihood, and $\beta f(m)$ is a penalty to guard against over

10 fitting. The BinSeg (binary segmentation) method starts with applying a single CP test statistic to the entire data set. If a CP is identified, the data are then split into two at the CP location. The single CP process is repeated for the two new data sets, before and after the change. If CPs are identified in either of the new data sets, they are split further. This procedure continues until no CPs are found in any parts of the data. This process is an approximate minimisation of (1) with $f(m) = m$, as any CP locations are conditional on CPs identified previously. The segment neighbourhood algorithm precisely minimises the

15 expression given by (1) using a dynamic programming technique to obtain the optimal segmentation for $(m + 1)$ CPs reusing the information calculated for m change points. The PELT (pruned exact linear time) method is similar to that of the segment neighbourhood algorithm in that it provides an exact segmentation. We have used the PELT algorithm instead of the segment neighbourhood method as it has proven to be more computationally efficient. The reason for this greater efficiency is the use of dynamic programming and pruning in the algorithm's construction.

20 A full description of these methods and the subroutines in R used in this study can be found in *Killick and Eckley (2014)*.

2.2.3 Estimation of the Lagrangian moisture transport from the main sources

In this study, we used a Lagrangian approach to calculate moisture transport from the main moisture sources as detected by *Vazquez et al. (2016)* (figure 1c) for the AR, AO, and its 13 subregions. This approach is based on the particle dispersion

25 model FLEXPART v9.0 (i.e., the FLEXible PARTicle dispersion model of Stohl and James (2004, 2005)) forced by ERA-Interim data from the ECMWF. This approach has been used extensively in moisture transport analysis *(e.g., Gimeno et al., 2010; 2013)*, and a review of its advantages and disadvantages versus other approaches for tracking water vapor was summarised by *Gimeno et al. (2012 and 2016)*. To briefly summarise this method, the atmosphere is divided into so-called particles (finite elements of volume with equal mass) and individual three-dimensional trajectories are tracked forward in time

30 for 10 days, the average residence time of water vapor in the atmosphere *(Numaguti, 1999)*. Then, taking into account the changes in (q) for each particle along its trajectory, the net rate of change of water vapour $(e - p)$ for every particle, $(e - p) = m(dq/dt)$, is estimated, with e and p representing evaporation and precipitation, respectively. The total atmospheric

moisture budget $(E - P)$ is estimated by adding up $(e - p)$ for all particles over a given area at each time step used in the analysis. To compute moisture transport for precipitation (MTP) from each source to each sink for the AO, the trajectories of particles from the moisture sources for the Arctic (AR) were followed forward in time from every source region detected by *Vazquez et al. (2016)* (figure 1c). This was done for 6 hours in the period 1980–2016. Then, we selected all particles losing

5   moisture, $(e - p) < 0$, at the sinks (whole Arctic or any of the sub-regions), and by adding $e - p$ for all of these particles, we estimated moisture transport for precipitation from the source to the sink $(E - P) < 0$ at daily, monthly or yearly scales. A schematic illustration of this approach is displayed in figure 2.

2.2.3 Identification of circulation types

10   The patterns of $(E - P) < 0$ can change daily in association with variations in atmospheric circulation. To evaluate the relationship between this variability and the moisture supply generated from each source of moisture, we identified different circulation types over the areas of interest using an applied methodology developed by *Fettweis et al. (2011)*. This approach consists of an automated circulation type classification based on a correlation analysis whereby atmospheric circulation is categorised into a convenient number of five discrete circulation types in the present study. For each pair of days, a similarity

15   index based on the Spearman rank correlation coefficient was calculated for the purpose of grouping days that showed similar circulation patterns *(Belleflamme et al., 2012)*. The first category contains the greatest number of similar days, where similarity is defined by a particular threshold (0.95 for the first class). After establishing the first class, the same procedure was applied for the remaining days using a lower similarity threshold to find the second and then all other classes. The complete procedure was repeated for different thresholds to optimise the percentage of variance explained (Philipp et al., 2010). This method is

20   termed a "leader" algorithm because each class is represented by a leader pattern considered as the reference day (Philipp et al., 2010). In this study, we used the geopotential height field at 850 hPa from ERA-Interim. Because our aim was to find and analyse different circulation patterns affecting the Arctic system linked to each source of moisture, the northern hemisphere from 20º to 90ºN was divided into sections according to the positions of the major sources of moisture (figure 1c). Thus, the circulation type classification was obtained seasonally for each of these sections.

3 Results

3.1 Climatological moisture transport for precipitation (MTP) to the Arctic region (AR) and Arctic Ocean (AO) subregions

30   Figure 3 displays the seasonal cycle of MTP to the AR from four major sources (Atlantic, Pacific, Siberia, and North America) and the relative contributions of each. MTP to the AR exhibits a marked seasonal cycle with a maximum in summer and a

minimum in winter; MTP doubles in the highest month (August) relative to the lowest month (February). The percentage of the contribution from each source is relatively constant throughout the year, with the Pacific, North America, Siberia, and the Atlantic contributing about 35%, 30%, 20%, and 15%, respectively.

The seasonal cycle is quite similar for eight of the 13 AO subregions (figure 4), with two other regions (Barents and the Central Arctic) exhibiting similar maxima, but with minima in May, and another (Chukchi) with two minima in March and November, and finally Greenland with a minimum in May but no clear maximum in summer, extending the typical summer high values to fall and winter (Greenland). The relative contributions of each moisture source are very diverse, with three general patterns: one with the a dominating closest source (a Pacific source for Bering, Chukchi, and Okhostk, a North American source for the Canadian Islands and Hudson, and a Siberian source for Kara and Laptev), another pattern where two sources share importance throughout the year (Atlantic and Siberian sources for Baffin and Greenland, and Pacific and North American sources for Beaufort), and a third where the Siberian source shares importance with two or more sources (Barents, Central Arctic, and East Siberia).

The relative importance of each ocean subregion on MTP to the AO (estimated as the sum of the 13 subregion) is shown in figure 5 where the percentage of moisture transport to the whole AO is displayed by region and month. There are four regions where the aggregated MTP received represent more than 60% of the MTP received for the whole Arctic. Those regions are Greenland, Baffin, Bering, and the Central Arctic, in order of importance. The contributions of Baffin, Bering, and the Central Arctic vary little throughout the year, representing about 20%, 12% and 10% of the MTP received for the whole Arctic, respectively, whereas the contribution of Greenland has a marked seasonal cycle with values around 25% for fall and winter, and 10–15% in spring and summer, seasons when two other sources gain importance, Hudson and Okhotsk, with percentages close to 10%. The almost constant contribution of Barents throughout the year is non-negligible, around 5%. The remaining sources have contributions less than 5%.

3.2 Moisture transport after and before Arctic sea ice change points

Figure 6 summarises the identified change points (CPs) in means identified using the AMOC method in the four series of whole Arctic sea ice extent anomalies (DS, MS, ADS, and AMS) from 1980 to 2016. DS only has CPs in the period from July to October; blue points therefore refer to the CPs in the daily series in this period. These CPs occurred mostly in 2004, the first part of September in 2006, and the last week of October in 2003. The results of both the BinSeg and PELT methods (results not shown) coincide for every day except for 17 September (2004 based on AMOC and 2006 for the other methods). The red bands in figure 6 portray the CPs in the MS data set (July–October). These CPs occurred in 2004 for July and September, a little earlier (2001) for August, and a little later (2005) for October. Both the BinSeg and PELT methods coincide in every month except for October (2005 based on AMOC and BinSeg, and 2006 for PELT). The green square corresponds to the CP in the 13,505-value series consisting of all days from 1 January 1980 to 31 December 2016 (ADS). The CP occurred on 22

September 2003, and was identified by the BinSeg, although not by PELT (the closest ones are 4 August 2002 and 26 January 2005). The purple line represents the CP in the 444-value series consisting of all months from January 1980 to December 2016 (AMS). This CP occurred in October 2003. The results of both the BinSeg and PELT methods coincide for this CP, and it is the only one for both. Overall, the results in figure 6 suggest that 2003 is the most appropriate year for analysis of differences

5   in moisture transport after and before a single CP date. The average values for ADS before/after the CP were 0.27/−0.91 and for AMS were 0.41/−0.74.

The top panel of Figure 7 portrays MTP from the four main Arctic moisture sources (figure 1c) until 2003 and from the following year (2004) onward for the AR, which includes continental and oceanic areas (figure 1a). The quantities in the plot result from averaging daily values of MTP. The statistical significance of the differences (table in figure 7 bottom) has been

10   estimated by comparing daily values of MTP before and after the CP, and the sample size is large enough (30 x 23 years vs 30 x 13 years) to permit application of the Student t-test. The pattern of changes in MTP before and after the change point for the AR shows no significant changes in late winter and spring, a significant decrease in MTP in summer, and increased MTP in fall and early winter, with the exception of October. The summer decrease is statistically significant (marked with blue crosses in the table of Figure 7) for the contributions of Pacific and Siberian sources throughout the entire summer, for the Atlantic

15   source in early summer, and for the North American source in late summer. The fall–early winter increase is statistically significant (red crosses) for the contributions of the North American source in three months (September, November, and December), for the Siberian and the Atlantic sources in two months (September and November; and October and December, respectively), and for the Pacific source only in one month (November).

However, because Arctic ice cover is extensive in geographical domain covering the subregion affected by very different

20   atmospheric circulation patterns, this pattern of change in MTP could not be homogeneous for the entire AO and its subregions. Finer-scale analysis can be done by restricting the analysis to oceanic areas only (the 13 Arctic oceanic subregions and the whole Arctic Ocean defined as the sum of these regions, figure 1b). The pattern of changes in MTP before and after the change point for the AO (figure 8 top left) is quite similar to the AR without significant changes in late winter and spring, with decreased MTP in summer and increased MTP in fall and early winter, now also including October. Small differences are

25   observed in the contributions of each source to the change of MTP toward the AO, with the Pacific source becoming much less important for the summer decrease and more important in the fall increased. The consistent increment is especially remarkable after the change point of MTP for all the moisture sources in September, the month when extension of Arctic sea ice is lowest.

The analysis by subregion allowed us to identify which subregions contributed most to change in MTP in the AO. As in the

30   case of the AR, the statistical significance of the differences (Table 1) has been estimated by comparing daily values of moisture transport before and after the CP. The diminished contribution of the Atlantic source to the AO in June and July is mainly attributed to the reduction of transport to Greenland; this decrease is not observed in August because of the compensation of the decrease to Greenland by the increase to Baffin. A moderate increase in October and a small decrease in December were also attributed to changes occurring in Greenland. The slightly decreased contribution of the Pacific to the AO in summer was

caused by the compensation of the decreased contribution of Bering (strong decrease) with a strong increase in the contribution of Okhotsk, with some influence of other regions such as Beaufort (decrease) and East Siberian (increase). There is greater concordance in fall and winter, with generally slight increments, which resulted in a small increase in the contribution of the Pacific to the AO. The greatly decreased contribution of the Siberian source to the AO in summer is attributed mainly to the

5   strong decrease of MTP to the Central Arctic and Laptev, and the generally slight increment of the contribution of the Siberian source for these regions in fall and early winter (with the exception of October); these changes result in similar behaviour for the AO. The different changes of the contribution of the North American source to the AO in July (increase) and August (decrease) reproduce the common changes observed in the contributions to Baffin and Hudson. The slight increase in contribution to the AO in September and October again is attributed to compensation of the increased to Hudson with a strong

10   decrease in September to the Canadian Islands and slight decreased in October to Baffin and Barents; the increased contribution of this source to the AO in December is the result of increased contribution to the Central Arctic and Barents, partially compensated by slight decrease to Hudson and Baffin.

3.3 Checking the Lagrangian results by analysing changes in vertical integrated moisture fluxes and atmospheric
15   **circulation patterns after and before Arctic sea ice change points**

It is useful to check the results derived from the Lagrangian approach to estimate MTP with other Eulerian approach such as the computation of vertical integrated moisture flux (VIMF). Supplemental figure S1 shows the climatological VIMF by month in the period from June to December (left panel) and the difference between the periods after the CP and before the CP for the zonal component (central panel) and the meridional component of VIMF (right panel). This methodology cannot estimate

20   specific changes in the MTP from each source to each sink as the more sophisticated Lagrangian approach does, but it is able to show whether patterns are compatible with the identified changes. For instance, in June (figure 9), the Atlantic source provides moisture for precipitation in the subregion of the Arctic Ocean named Greenland in our study, as revealed by the flux vectors in the top panel. However, the track of moisture from the source to the sink is clearly difficulted for the period after the CP relative to the period before the CP, as revealed by negative values of the zonal component (blue colours in middle

25   figure 9) in the band 45–60ºN latitude (less moisture transported from west to east, the direction of the source–receptor path) and negative values of meridional winds (blue colours in bottom figure 9) in the band 20–60ºW longitude (less moisture transported from south to north, the direction of the source–receptor path). We have done this analysis for each month, and for source and sink areas, and the patterns can explain all the significant results found in the Lagrangian analysis with almost absolute agreement (figure S1).

30   An additional demonstration of the robustness of these results can be derived by analysing the changes in atmospheric circulation responsible for changes in moisture transport. Changes in MTP may be related either to alterations in moisture sources caused by changes in circulation patterns, or to changes in the intensity of the moisture sources because of enhanced evaporation, or to a combination of these two mechanisms. At a daily scale, changes in intensity are negligible, but changes in

circulation may be significant. Thus, to analyse whether there are important differences in MTP from sources to sinks associated with different circulation patterns, and how such differences could affect MTP in the AR, we grouped individual days into four circulation types using the methodology developed by *Fetttweis et al. (2011)* and explained in the Data and Methods sections. We have separated the analysis into four sectors centred on the four sources of moisture to the AR to filter out annular effects, as we are interested in regional influences.

Supplemental figure S2 shows the summer and fall types of circulation centred on the four source areas (Atlantic, Pacific, Siberia, and North America), with each individual map representing the anomalies of geopotential height at 850 hPa (Z850) for the four different classes found (from CTC1 to CTC4, with the percentage of days grouped). The average MTPs for each class before and after the CP are summarised in Table S1, whereas changes in the frequency of each class before and after the CP are shown in Table S2. One of these sectors and one season can serve us as an example of these results: the Atlantic during summer (figure 10). The anomalies of geopotential height at 850 hPa (Z850) for the four different classes found (figure 10 top) show patterns that resemble the known teleconnection patterns in the region (*Barnston and Livezey, 1987* and http://www.cpc.ncep.noaa.gov/data/teledoc/telecontents.shtml). Thus, CTC1 has a zonal dipolar structure that resembles the positive phase of the East Atlantic pattern, closely related to enhanced precipitation on Greenland; CTC2 is slightly similar to the negative phase of the East Atlantic/western Russia, associated with enhanced precipitation on Barents; CTC3 resembles the negative phase of the North Atlantic Oscillation, related to diminished precipitation on Greenland and enhanced precipitation on Barents, and CTC4 is similar to the positive phase of the Scandinavian pattern associated with diminished precipitation on Barents. The middle panel of figure 10 shows the average MTP for each class in the summer months from the Atlantic source to the AO (dark blue line) and the two dominant subregions, Barents and Greenland (light blue and orange lines, respectively). CTC1 is the circulation type responsible for the highest MTP in the three summer months, and CTC3 and CTC4 are responsible for the lowest MTP, depending on the month. The change of frequency of these classes representing circulation types before and after the CP (Figure 10 bottom) shows a decrease of the days belonging to CTC1, with the highest MTP from 40 to 25.4 days, and an increase of days belonging to CTC3 (from 9.58 to 15.15) and CTC4 (from 4.62 to 5.85), the two classes with the lowest MTP. These results are absolutely consistent with our Lagrangian results of changes in MTP. A similar analysis to the one for this sector, moisture source region, and season can be done for all the significant results found in the Lagrangian analysis with very good agreement.

4 Conclusions

The perfect pattern of MTP for Arctic sea ice melting consists of a general decrease in moisture transport in summer and an increase in fall and early winter, with different contributions depending on the moisture source and ocean subregion. This pattern is not only statistically significant but also consistent with Eulerian flux diagnosis, changes in circulation type frequency, and known mechanisms affecting snowfall or rainfall on ice in the Arctic. The consistent increment after the CP of

MTP for all moisture sources in September, the month when extension of Arctic sea ice is lowest, is particularly remarkable. Thus, it is clear beyond doubt that an increment in moisture transport during this month favours ice melting, regardless of the source of moisture.

These results suggest that ice-melting at a multiyear scale is favoured by a decrease in moisture transport in summer and an increase in fall and early winter. These results are notable because of their consistence with mechanisms related to precipitation and ice cover. It is important to note that we have estimated MTP such that so any relationship of our results with sea ice must be interpreted in terms of changes in precipitation caused by changes in moisture transport and the effect of precipitation on ice cover. Snowfall is the dominant (almost unique) form of precipitation during most of the year, with the exception of late summer. As noted in the introduction, when precipitation is produced in the form of snowfall on sea ice, it enhances thermal insulation, and reduces sea ice growth in winter *(Leppäranta, 1993),* but increases the surface albedo, and thus reduces melt in spring and summer *(Cheng et al., 2008).* These phenomena justify the opposite change in moisture transport for fall and winter versus spring. However, in late summer and early fall, precipitation as rain gains importance, and rainfall is generally related to sea ice melting.

The results of this paper also reveal another important conclusion: the assumed and partially documented enhanced poleward moisture transport from lower latitudes as a consequence of increased moisture from climate change *(Zhang et al., 2013)* has not been simple or constant in its links with enhanced Arctic precipitation throughout the year in the present climate. Major moisture sources for the Arctic did not provide more moisture for precipitation to the Arctic in summer after 2003, the change point (CP) for Arctic sea ice, than before, although they did provide more moisture in fall and early winter. Because the enhanced Arctic precipitation projected by most models for the end of the century *(Bintaja and Selten, 2014)* is partly attributed to enhanced poleward moisture transport from latitudes lower than 70ºN *(Bintanja and Andry, 2017),* where the major sources studied herein are located, our results raise questions of whether this change has occurred so simply in the current climate, and these questions merit further study.

Acknowledgements

The authors acknowledge funding by the Spanish government within the EVOCAR (CGL2015-65141-R) project, which is also funded by FEDER (European Regional Development Fund). The data used are listed in the references, tables and supplements.

References

Årthun, M., Eldevik, T., Smedsrud, L. H., Skagseth, Ø, & Ingvaldsen, R. B. (2012). Quantifying the influence of Atlantic heat on Barents Sea ice variability and retreat, *Journal of Climate*, *25*(13), 4736–4743, https://doi.org/10.1175/JCLI-D-11-00466.1.

Barnston, A. G., & Livezey, R. E. (1987). Classification, seasonality and persistence of low-frequency atmospheric circulation patterns. *Monthly Weather Review*, *115*, 1083-1126, doi.org/10.1175/1520-0493(1987)115<1083:CSAPOL>2.0.CO;2

Belleflamme A., Fettweis, X., Lang, C., & Erpicum, M. (2012). Current and future atmospheric circulation at 500 hPa over Greenland simulated by the CMIP3 and CMIP5 global models. *Climate Dynamics, 41*, 2061-2080, doi.org/10.1007/s00382-012-1538-2

Bintaja R. & Andry O. (2017). Towards a rain-dominated Arctic. *Nature Climate Change 7,* 263–267, https://doi.org/10.1038/nclimate3240.

Bintaja R. & Selten F. M. (2014). Future increases in Arctic precipitation linked to local evaporation and sea-ice retreat. *Nature 509*, 479–482. doi.org/10.1038/nature13259

Cheng, B., Zhang, Z., Vihma, T., Johansson, M., Bian, L., Li, Z., & Wu, H. (2008). Model experiments on snow and ice thermodynamics in the Arctic Ocean with CHINARE2003 data. *Journal of Geophysical Research*, *113*, C09020, doi.org/10.1029/2007JC004654

Cohen, J., Screen, J. A., Furtado, J. C., Barlow, M., Whittleston, D., Coumou, D., Jones, J. (2014). Recent Arctic amplification and extreme mid-latitude weather. *Nature Geoscience, 7,* 627–637, doi.org/10.1038/ngeo2234.

Dee, D. P., Uppala, S. M., Simmons, A. J., Berrisford, P., Poli, P., Kobayashi, S. Vitart, F. (2011). The ERA-Interim reanalysis: Configuration and performance of the data assimilation system *Quarterly Journal of the Royal Meteorological Society*, *137*(656), 553–597, doi.org/10.1002/qj.828.

Ding, Q., Schweiger, A., L'Heureux, M., Battisti, D. S., Po-Chedley, S., Johnson, N. C., … Steig, E. J. (2017). Influence of high-latitude atmospheric circulation changes on summertime Arctic sea ice, *Nature Climate Change*, *7*, 289–295, doi.org/10.1038/nclimate3241.

Fetterer F., Knowles K., Meier W., & Savoie M. (2016, updated daily). Sea Ice Index, Version 2. [1979-2016]. Boulder, Colorado USA. NSIDC: National Snow and Ice Data Center. doi: /dx.doi.org/10.7265/N5736NV7. (last accessed 22 November 2017).

Fettweis, X., Mabille, G., Erpicum, M., Nicolay, S., & Van den Broeke, M. (2011). The 1958–2009 Greenland ice sheet surface melt and the mid-tropospheric atmospheric circulation. *Climate Dynamics, 36*, 139-159,, doi.org/10.1007/s00382-010-0772-8

Gimeno, L., Dominguez, F., Nieto, R., Trigo, R. M., Drumond, A., Reason, C., Marengo, J. (2016). Major Mechanisms of Atmospheric Moisture Transport and Their Role in Extreme Precipitation Events. *Annual Review of Environment and Resources*, *41*, 117–141, doi.org/10.1146/annurev-environ-110615-085558.

Gimeno, L., Drumond, A., Nieto, R., Trigo, R. M., & Stohl, A. (2010). On the origin of continental precipitation. *Geophysical Research Letters*, *37,* doi.org/10.1029/2010GL043712

Gimeno, L., Nieto, R., Drumond, A., Castillo, R., & Trigo, R.M. (2013). Influence of the intensification of the major oceanic moisture sources on continental precipitation. *Geophysical Research Letters*, *40*, 1443–1450,, doi.org/10.1002/grl.50338

Gimeno, L., Stohl, A., Trigo, R .M., Domínguez, F., Yoshimura, K., Yu, L., … Nieto, R. (2012). Oceanic and Terrestrial Sources of Continental Precipitation. *Reviews of Geophysics*, *50*, RG4003, doi.org/10.1029/2012RG000389

Gimeno, L., Vázquez, M., Nieto, R., & Trigo, R. M. (2015). Atmospheric moisture transport: the bridge between ocean evaporation and Arctic ice melting. *Earth System Dynamics, 2, 583-589,* doi.org/10.5194/esd-6-583-2015.

5 Graversen, R. G., & Burtu, M. (2016). Arctic amplification enhanced by latent energy transport of atmospheric planetary waves, *Quarterly Journal of the Royal Meteorological Society*, *142*(698), 2046–2054, doi.org/10.1002/qj.2802.

Graversen, R. G., Mauritsen, T., Drijfhout, S., Tjernström, M., & Mårtensson, S. (2011). Warm winds from the Pacific caused extensive Arctic sea-ice melt in summer 2007. *Climate Dynamics, 36(*11), 2103–2112, doi:10.1007/s00382-010-0809-z.

IPCC: Climate Change (2013). The physical science basis, in: Contribution of working group 1 to the fifth assessment report

10 of the intergovernmental panel on climate change. Edited by: Stocker, T. F., Qin, D., Planttner, G. K., Tignor, M., Allen, S. K., Boschung, J., Nauels, A., Xia, Y., Bex, V., and Midgley, P. M., Cambridge University Press, Cambridge, UK and New York, NY, USA,.

Jakobson, E., Vihma, T., Palo, T., Jakobson, L., Keernik, H., & Jaagus, J. (2012). Validation of atmospheric reanalyses over the central Arctic Ocean, *Geophysical Research Letters*, *39*, L10802, doi.org/10.1029/2012GL051591.

15 Kapsch, M.-L., Graversen, R. G., & Tjernstrom, M. (2013). Springtime atmospheric energy transport and the control of Arctic summer sea-ice extent. *Nature Climate Change*, *3*(8), 744–748. doi.org/10.1038/nclimate1884

Killick, R., & Eckley, I. (2014). changepoint: An R Package for changepoint analysis. *Journal of Statistical Software 58*, 1–15, https://doi.org/ 10.18637/jss.v058.i03

Koenigk, T., Brodeau, L., Graversen, R. G., Karlsson, J., Svensson, G., Tjernström, M., … Wyser, K. (2013). Arctic climate

20 change in the 21st century in an ensemble of AR5 scenario projections with EC-Earth. *Climate Dynamics, 40*, 2719–2743, doi.org/10.1007/s00382-012-1505-y.

Lee, H. J., Kwon, M. O., Yeh, S.-W., Kwon, Y.-O., Park, W., Park, J.-H., … Alexander, M. A. (2017). Impact of Poleward Moisture Transport from the North Pacific on the Acceleration of Sea Ice Loss in the Arctic since 2002. *Journal of Climate*, *30*(17), 6757-6769, doi.org/10.1175/JCLI-D-16-0461.1

25 Leppäranta, M. (1993). A review of analytical models of sea-ice growth, *Atmosphere-Ocean, 31*(1), 123–138. doi.org/10.1080/07055900.1993.9649465

Lorenz, C., & Kunstmann, H. (2012). The hydrological cycle in three state-of-the-art reanalyses: Intercomparison and performance analysis. *Journal of Hydrometeorology, 13*, 1397–1420, doi.org/10.1175/JHM-D-11-088.1

Mortin, J., Svensson, G., Graversen, R. G., Kapsch, M.-L., Stroeve, J. C., & Boisvert, L. N. (2016). Melt onset over Arctic

30 sea ice controlled by atmospheric moisture transport. *Geophysical Research Letters*, *43*, 6636–6642, doi.org/10.1002/2016GL069330.

Numaguti, A. (1999). Origin and recycling processes of precipitating water over the Eurasian continent: Experiments using an atmospheric general circulation model, *Journal of Geophysical Research*, *104*, 1957–1972, doi.org/10.1029/ 1998JD200026

Ogi, M., & Wallace, J. M. (2007). Summer minimum Arctic sea ice extent and the associated summer atmospheric circulation. *Geophysical Research Letters, 34*, L12705, doi.org/10.1029/2007GL029897.

Park, H.-S., Lee, S., Son, S.-W., Feldstein, S. B., & Kosaka, Y. (2015a). The impact of poleward moisture and sensible heat flux on Arctic winter sea ice variability. *Journal of Climate*, *28*(13), 5030–5040, doi.org/10.1175/JCLI-D-15-0074.1.

Park, H.-S., Lee, S., Kosaka, Y., Son, S.-W., & Kim, S.-W. (2015b). The impact of Arctic winter infrared radiation on early summer sea ice. *Journal of Climate*, *28*(15), 6281–6296, doi.org/10.1175/JCLI-D-14-00773.1.

Philipp, A., Bartholy, J., Beck, C., Erpicum, M., Esteban, P., Fettweis, X., S. Tymvios (2010). COST733CAT—a 787 database of weather and circulation type classifications, *Physics and Chemistry of the Earth, 35*(9–12), 788 360–373, doi.org/10.1016/j.pce.2009.12.010

Post, E., Bhatt, U. S., Bitz, C. M., Brodie, J. F., Fulton, T. L., Hebblewhite, M., Walker, D. A. (2013). Ecological consequences of sea-ice decline. *Science, 341*, 519–524 (2013). doi.org/10.1126/science.1235225

Rigor, I. G., Wallace, J. M., & Colony, R. L. (2002). Response of sea ice to the Arctic Oscillation. *Journal of Climate, 15*, 2648–2663, https://doi.org/10.1175/1520-0442. (2002)015<2648:ROSITT>2.0.CO;2.

Rinke, A., Maturilli, M., Graham, R. M., Matthes, H., Handorf, D., Cohen, L., Moore, J. C. (2017). Extreme cyclone events in the Arctic: Wintertime variability and trend. *Environmental Research Letters, 12,* 094006, doi.org/10.1088/1748-9326/aa7def

Screen, J. A., & Simmonds, I. (2010). The central role of diminishing sea ice in recent Arctic temperature amplification. *Nature, 464*, 1334-1337, doi.org/10.1038/nature09051.

Stohl, A., & James, P. (2004). A Lagrangian analysis of the atmospheric branch of the global water cycle. Part I: Method description, validation, and demonstration for the August 2002 flooding in central Europe. *Journal of Hydrometeorology, 5*, 656–678, https://doi.org/10.1175/1525-7541(2004)0052.0.CO;2.

Stohl, A., & James, P. (2005). A Lagrangian analysis of the atmospheric branch of the global water cycle. Part II: Moisture transports between the Earth's ocean basins and river catchments, *Journal of Hydrometeorology, 6*, 961–984, doi.org/10.1175/JHM470.1.

Tang, Q., Zhang, X., & Francis, J. A. (2014). Extreme summer weather in northern mid-latitudes linked to a vanishing cryosphere. *Nature Climate Change, 4*, 45–50, doi.org/10.1038/nclimate2065.

Tjernström, M., Shupe, M. D., Brooks, I. M., Persson, P. O. G., Prytherch, J., Salisbury, D. J., … Wolfe, D. (2015). Warm-air advection, air mass transformation and fog causes rapid ice melt. *Geophysical Research Letters, 42*, 5594–5602, doi.org/10.1002/2015GL064373.

Vázquez, M., Nieto, R., Drumond, A., & Gimeno, L. (2016). Moisture transport into the Arctic: Source-receptor relationships and the roles of atmospheric circulation and evaporation. *Journal of Geophysical Research: Atmospheres, 121,* doi.org/10.1002/2016JD025400.

Vihma, T., J. Screen, M. Tjernström, B. Newton, X. Zhang, V. Popova, C. Deser, M. Holland, and T. Prowse (2016), The atmospheric role in the Arctic water cycle: A review on processes, past and future changes, and their impacts, *J. Geophys. Res. Biogeosci.,* 121, 586–620, doi:10.1002/2015JG003132.

Woods, C., & Caballero, R. (2016). The role of moist intrusions in winter Arctic warming and sea ice decline, *Journal of Climate*, *29*(12), 4473–4485, doi.org/10.1175/JCLI-D-15-0773.1.

Woods, C., Caballero, R., & Svensson, G. (2013). Large-scale circulation associated with moisture intrusions into the Arctic during winter. *Geophysical Research Letters*, *40*, 4717–4721, doi.org/10.1002/grl.50912.

5   Zhang, Y., Maslowski, W., & Semtner, A. J. (1999). Impact of mesoscale ocean currents on sea ice in high-resolution Arctic ice and ocean simulations. *Journal of Geophysical Research*, *104*(C8), 18,409–18,429, doi.org/10.1029/1999JC900158.

Zhang, X., He, J., Zhang, J., Polyakov, I., Gerdes, R., Inoue, J., & Wu, P. (2012). Enhanced poleward moisture transport and amplified northern high-latitude wetting trend. *Nature Climate Change, 3*, 47–51, doi.org/10.1038/nclimate1631.
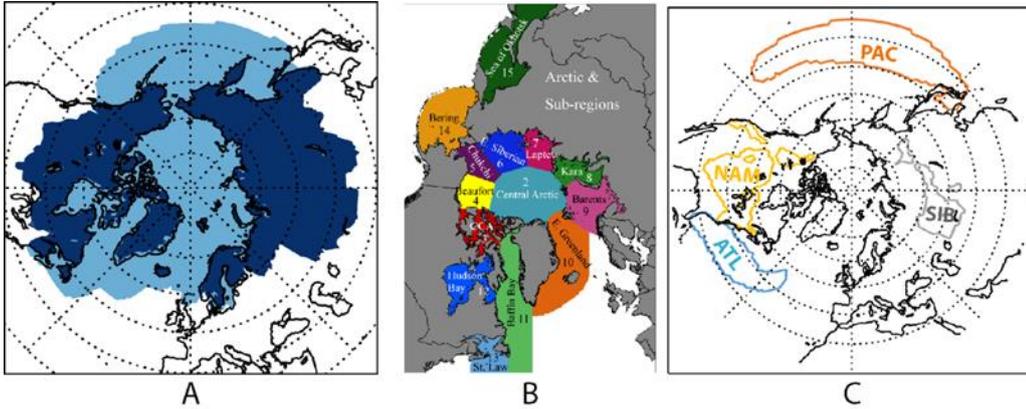
Figure 1. A) The Arctic region (AR) included in the present work defined following the definition of Roberts et al. (2010). B) The Arctic Ocean (OA) and its 13 subregions as described by Boisvert et al. (2015). C) Major moisture sources for the Arctic as detected by Vazquez et al. (2016).
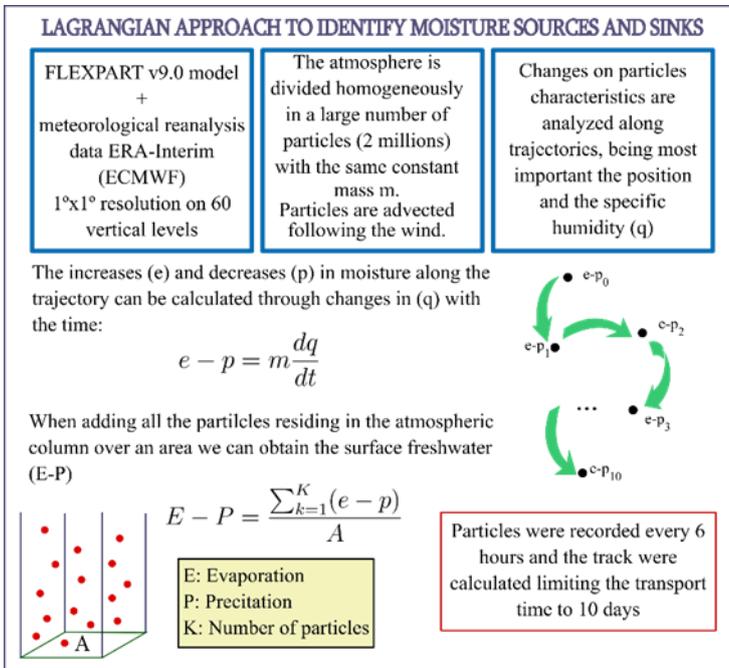
Figure 2. A scheme of the Lagrangian approach used to estimate moisture transport.
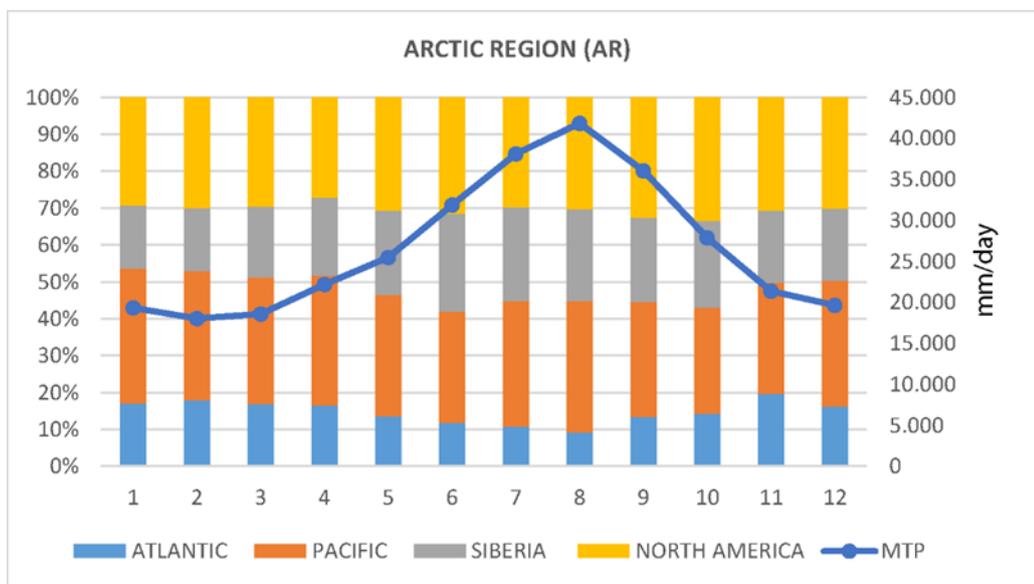
5   **Figure 3. Seasonal cycle of moisture transport for precipitation (MTP) to the Arctic region (AR) from the four major sources (Atlantic, Pacific, Siberia, and North America). Values at the right represent absolute values of transport, and those at the left indicate the relative contribution of each source by percentage.**

Figure 4. Same as in figure 3, but for each of the 13 subregions of the Arctic Ocean (AO).
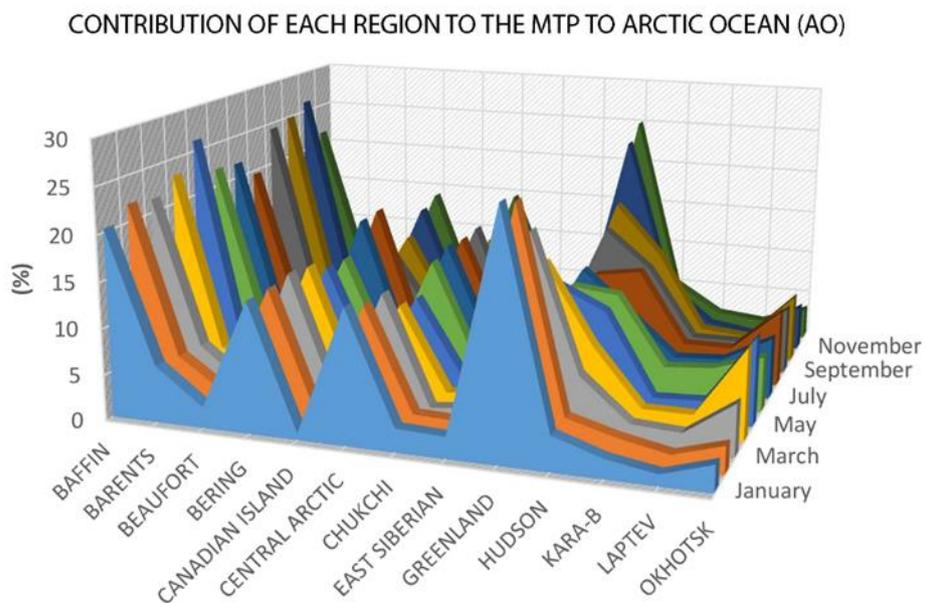
5   **Figure 5. Percentage of moisture transport for precipitation to the whole Arctic Ocean by subregion and month.**
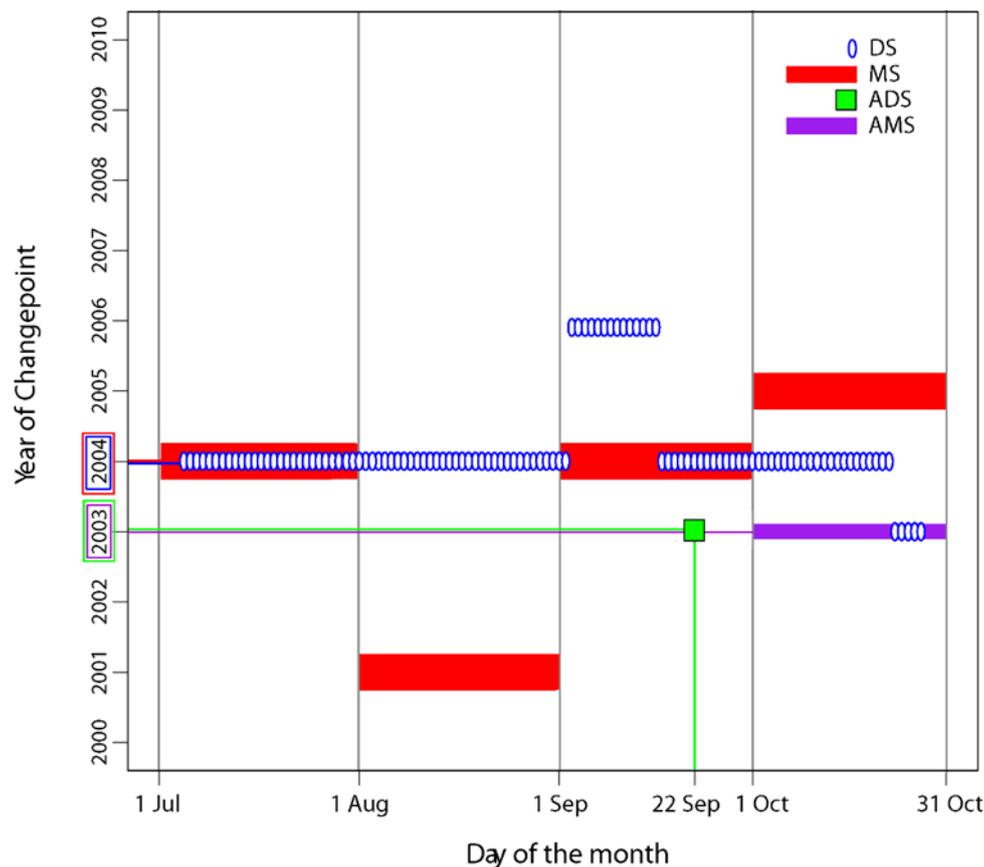
5 **Figure 6. Summary of the identified change points (CPs) in means identified using the AMOC method with the four series of ice extent anomalies for the whole Arctic (DS, MS, ADS, and AMS) from 1980 to 2016. The blue points refer to the change points in DS; the red lines portray change points in the MS (July–October). The green square corresponds to the change point in the ADS, and the purple line represents the change point in the AMS.**

	Jan	Feb	Mar	Apr	May	Jun	Jul	Aug	Sep	Oct	Nov	Dec
ATLANTIC SOURCE				X	X	X		X		X		X
PACIFIC SOURCE				X		X	X	X			X	
SIBERIAN SOURCE			X	X	X	X	X	X	X		X	
NORTH AMERICA SOURCE	X	X	X				X	X	X		X	X
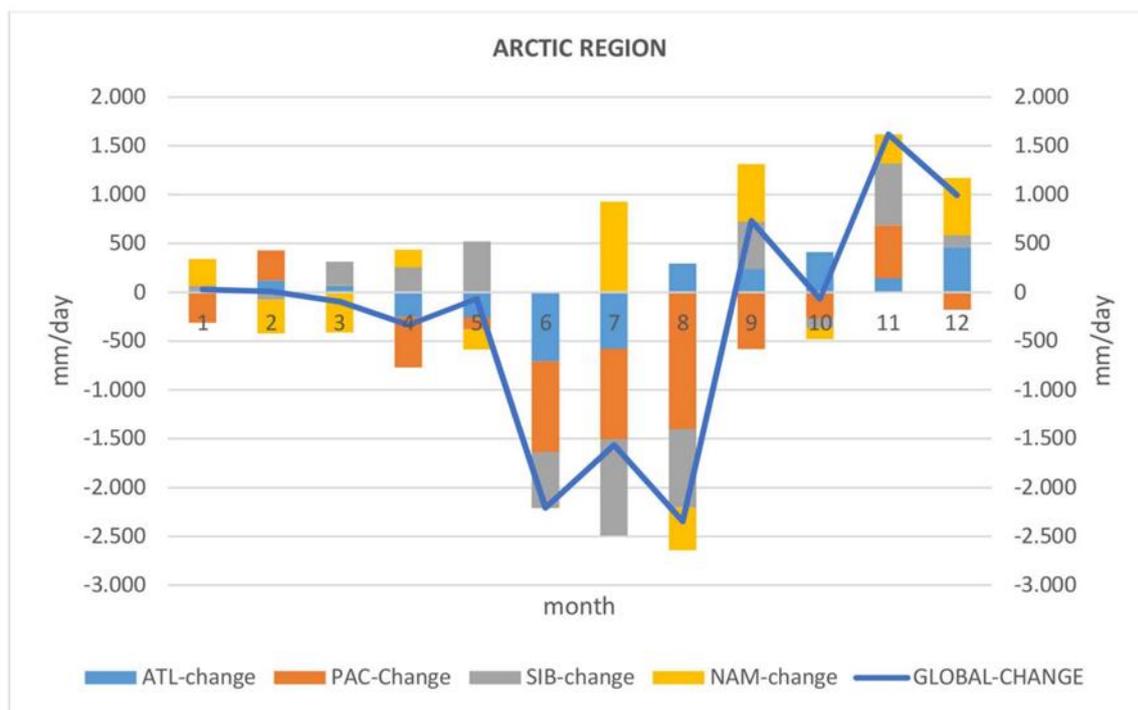
Figure 7. (top) Moisture transport for precipitation (MTP) from the four main Arctic moisture sources until 2003 (change point, CP) and from the following year onward for the Arctic region (AR); (bottom) summary of the statistical significance of the differences estimated by comparing daily values of moisture transport before and after the CP, based on the Student *t*-test. Red crosses indicate statistical significance at the 95% confidence level for increases after the CP; blue crosses indicate statistical significance at the 95% confidence level for decreases after the CP
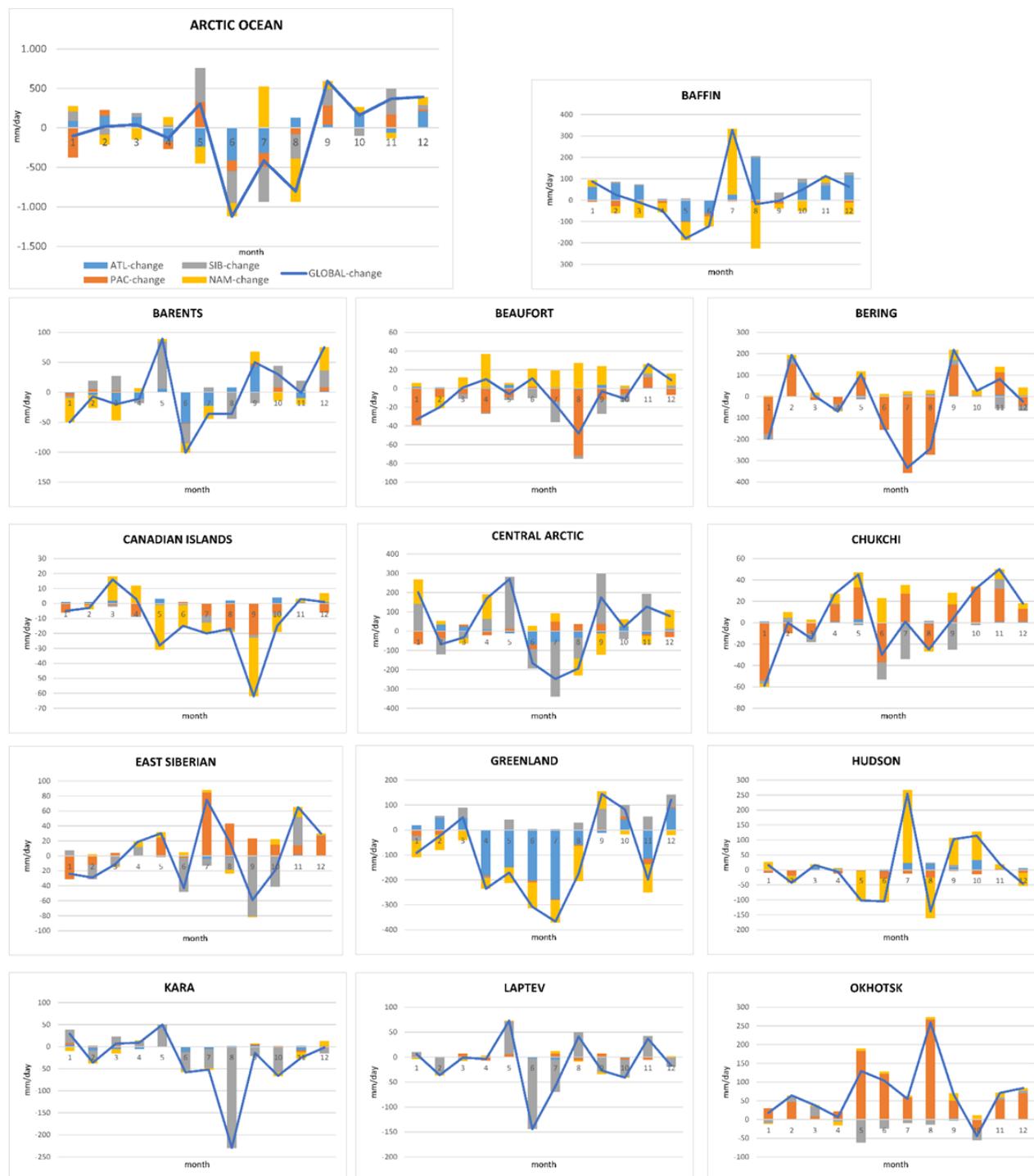
Figure 8. As figure 7 for the Arctic Ocean (AO) and its 13 subregions.
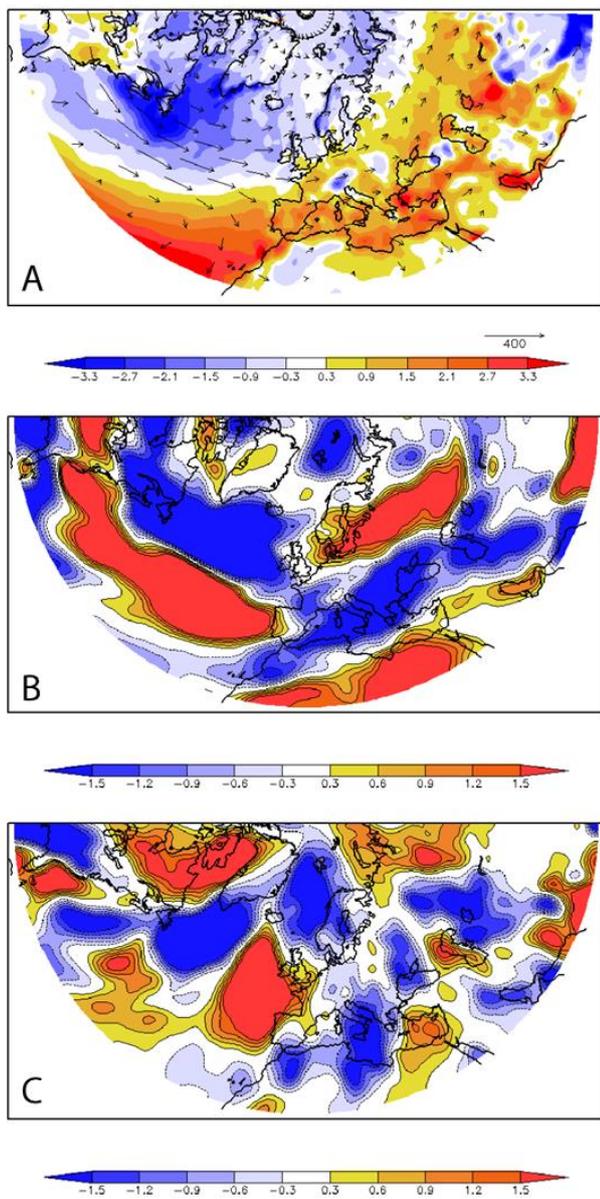
Figure 9. A) The climatological vertical integrated moisture flux (VIMF) (vector, kg/m/s) and its divergence (shaded, mm/yr) in June for the European sector, B) the difference between the periods after vs before the CP for the zonal component of VIMF, and C) as for b but for the meridional component of VIMF.
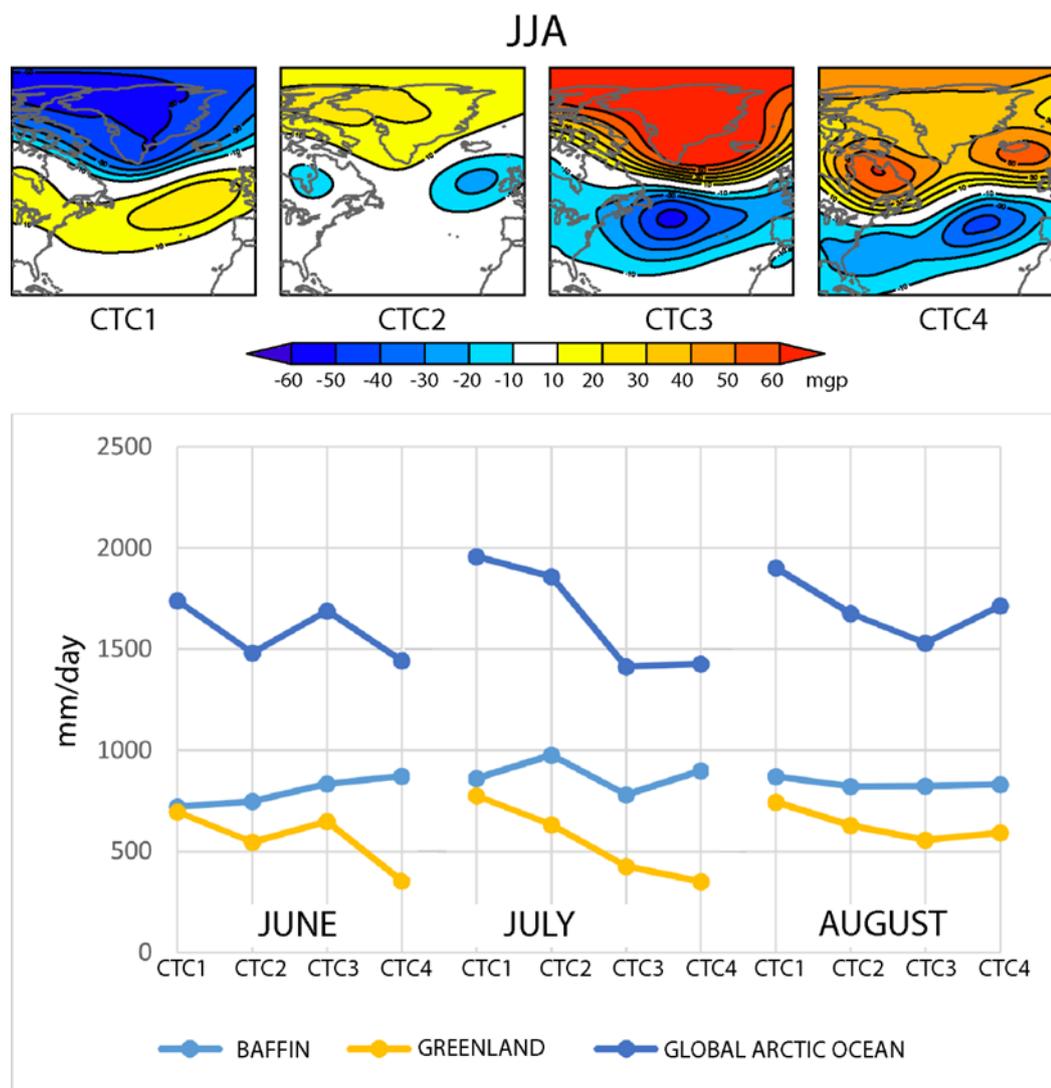
Figure 10. (top) Anomalies of geopotential height at 850 hPa (Z850) for the four types of circulation centred in the Atlantic sector in summer (classes CTC1 to CTC4), and the percentages of days grouped in each class. **(middle)** Average moisture transport for precipitation (MTP) for each class and summer months from the Atlantic source to the Arctic Ocean (AO), and the two dominant subregions, Barents and Greenland. **(bottom)** Change of frequency of these circulation types (classes) before and after the change point.

ATLANTIC SOURCE	Jan	Feb	Mar	Apr	May	Jun	Jul	Aug	Sep	Oct	Nov	Dec
Baffin			X		X			X				X
Barents			X			X	X		X			
Beaufort	X		X		X				X	X	X	X
Bering		X	X		X		X		X		X	X
Canadian	X	X	X		X			X		X		X
Central Arctic		X	X			X	X	X		X		
Chukchi	X				X			X	X		X	X
East Siberian		X			X	X	X	X			X	
Greenland				X	X	X	X				X	X
Hudson			X				X	X		X		
Kara	X	X	X	X		X					X	
Laptev	X	X				X	X	X		X		X
Okhotsk		X				X		X	X		X	X

PACIFIC SOURCE	Jan	Feb	Mar	Apr	May	Jun	Jul	Aug	Sep	Oct	Nov	Dec
Baffin		X		X		X		X				
Barents	X								X	X		X
Beaufort	X			X				X			X	
Bering	X	X				X	X	X	X		X	
Canadian	X			X			X	X	X	X		X
Central Arctic	X	X										
Chukchi	X				X	X				X	X	
East Siberian	X				X		X	X	X	X		X
Greenland	X	X		X		X		X		X		X
Hudson		X		X		X	X	X		X		X
Kara	X	X	X						X	X	X	
Laptev			X	X	X			X	X	X	X	
Okhotsk	X	X			X		X	X			X	X

SIBERIAN SOURCE	Jan	Feb	Mar	Apr	May	Jun	Jul	Aug	Sep	Oct	Nov	Dec
Baffin		X	X		X			X	X	X	X	X
Barents			X		X			X		X		X
Beaufort			X		X	X	X		X	X	X	
Bering	X	X		X	X				X		X	X
Canadian			X	X			X		X	X	X	
Central Arctic	X	X					X		X		X	
Chukchi			X			X	X		X		X	
East Siberian		X	X			X			X	X	X	
Greenland	X		X		X			X	X	X	X	X
Hudson	X	X	X					X	X	X	X	X
Kara	X	X	X		X			X		X		X
Laptev	X	X			X	X	X		X		X	X
Okhotsk	X	X	X		X	X			X			

NORTH AMERICA SOURCE	Jan	Feb	Mar	Apr	May	Jun	Jul	Aug	Sep	Oct	Nov	Dec
Baffin			X		X		X	X				X
Barents	X		X			X	X		X			X
Beaufort			X	X			X	X			X	X
Bering		X			X	X	X		X	X	X	X
Canadian			X	X	X	X			X			
Central Arctic	X			X				X	X			X
Chukchi				X	X	X	X		X		X	
East Siberian				X	X					X	X	
Greenland					X	X	X	X			X	
Hudson		X			X		X	X	X	X		X
Kara	X	X	X			X				X	X	X
Laptev	X		X				X		X			X
Okhotsk		X	X		X	X			X	X	X	X

Table I. Summary of the statistical significance of the MTP differences estimated by comparing daily values of moisture transport before and after the CP, based on the Student t-test. Red crosses indicate statistical significance at the 95% confidence level for increases after the CP; blue crosses indicate statistical significance at the 95% confidence level for decreases after the CP.